Fully Integrated Solid-State LiDAR Transmitter on a Multi-Layer Silicon-Nitride-on-Silicon Photonic Platform

Weihan Xu[1], Yuyao Guo[1], Xinhang Li[1], Chuxin Liu[1], Liangjun Lu[1, 2, *], Jianping Chen[1, 2], and Linjie Zhou[1, 2]
[1]*State Key Laboratory of Advanced Optical Communication Systems and Networks, Shanghai Key Lab of Navigation and Location Services, Shanghai Institute for Advanced Communication and Data Science, Department of Electronic Engineering, Shanghai Jiao Tong University, Shanghai 200240, China*
[2]*SJTU-Pinghu Institute of Intelligent Optoelectronics, Pinghu 314200, China*
**luliangjun@sjtu.edu.cn*

Abstract: We demonstrated a LiDAR transmitter incorporating both a hybrid-integrated tunable external cavity laser and a high-resolution 2-D optical phased array beam-steerer on a tri-layer silicon-nitride-on-silicon photonic platform. © 2022 The Authors

1. Introduction

Ever since 2009 [1], photonic integration has been innovating towards the realization of chip-scale LiDARs with inertial-free beam-steering and a sufficient power budget. Solid-state beam-steering technologies, especially optical phased arrays (OPAs) [2], are under active investigation while heterogeneous [3] or hybrid-integrated [4, 5] laser sources have been demonstrated for fully-integrated transmitters. With the rapid development of silicon nitride (Si_3N_4)-on-silicon photonic platform [6], new opportunities emerge where the merits of silicon-nitride including high-power handling [7], low insertion loss, and robustness to temperature variation [8] can be combined with the traditional advantages of silicon such as high mode confinement and efficient thermo-optic (TO) tuning. To date, a variety of OPAs have been implemented on this platform either with Si_3N_4-based power splitting [7, 9] or Si-Si_3N_4 hybrid grating antenna [9], leveraging on certain aspects of the aforementioned potentials.

Here, we report a fully integrated LiDAR transmitter (Tx) based on this platform [6]. The device comprises a widely tunable (~100 nm) external cavity laser (ECL) of a narrow linewidth (2.8 kHz) and a wavelength-assisted 2-D beam-steerer based on a 256-channel aperiodic OPA. Thanks to the high-power handling of the Si_3N_4 external cavity, an on-chip lasing output of 12.6 dBm is achieved. In addition, the small TO coefficient of Si_3N_4 suppresses the inter-channel crosstalk originated from the phase-tuning-induced thermal gradient, resulting in high fidelity beam-steering. The device exhibits an on-chip insertion loss below 3 dB together with a platform-record beam divergence of 0.047°×0.034° measured in full-width at half maximum (FWHM) in the phased array scanning axis (θ) and the wavelength scanning axis (ψ) respectively without applying special processing techniques as reported in prior arts.

2. Chip Design

With key components shown in Figs. 1 (a-c), the fully integrated LiDAR transmitter adopts laser input either from a remote laser source coupled through the fiber array (FA) or from the on-chip ECL selected by the Si_3N_4 Mach–Zehnder interferometer (MZI) switch. The optical power is then split into 256 channels by 8 stages of cascaded Si_3N_4-based 1×2 multimode interferometers (MMIs) for element-wise phase control and optical path difference (OPD) compensation. Finally, the optical wave radiates into the free-space through the grating antennas, forming a far-field pattern of high directivity via construction interference. All Tx functionalities expect for laser gain are integrated in a single PIC. In addition, to fully exploit the merits of silicon nitride waveguides (WGs), silicon waveguides are used only for TO phase tuning, OPD compensation, and grating antennas in the emitter array as illustrated in Fig. 1 (e). Since silicon waveguides reside strictly after the power splitting and are not used for resonant structures inside the laser cavity, the nonlinear effects (such as two-photon absorption and the subsequent free-carrier absorption) are of no significance.

More specifically, Fig. 1 (a) shows the schematic of the hybrid-integrated ECL, consisting of a Si_3N_4 wavelength-selective reflector and a co-packaged reflective semiconductor optical amplifier (RSOA). The rear side of the RSOA is high reflection (HR) coated acting as one mirror of the laser cavity. The InP waveguide on the front side is slanted by 8° and anti-reflection (AR) coated to reduce reflectivity. The Si_3N_4 circuit consists of a spot-size converter (SSC), a thermo-optic phase shifter (PS), a two-ring-based Vernier filter, and a tunable Sagnac loop reflector (TSL). The free spectral range (FSR) of the two rings are designed as 2.179 nm and 2.132 nm, respectively, and the FSR of the Vernier filter thus obtained is about 100 nm.

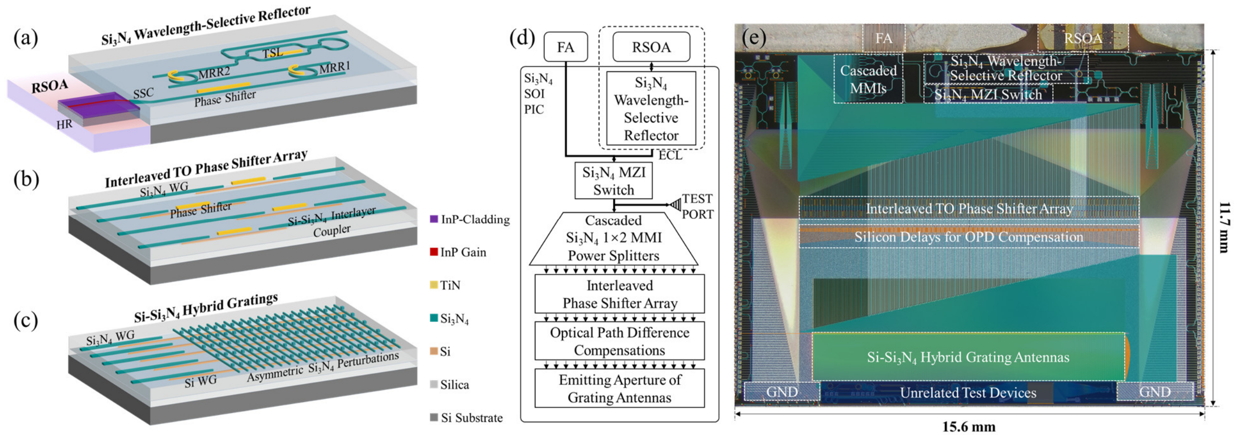

Fig. 1 (a-c) Schematics of (a) the hybrid-integrated external cavity laser (ECL), (b) the interleaved TO phase shifter array for beamforming and beam-steering, (c) the aperiodic Si-Si_3N_4 hybrid grating array. (d) Schematic and (e) photo of the assembled chipset consisting of a fiber array (FA), a reflective semiconductor optical amplifier (RSOA), and the tri-layer Si_3N_4-on-Si photonic integrated circuit (PIC) in a single chip.

For the OPA, by adopting an interleaved Si-Si_3N_4 TO phase shifter array as shown in Fig. 1 (b), thermal crosstalk to the adjacent channels from the TO phase shifter is greatly reduced due to the significant TO coefficient difference between the Si_3N_4 WG (dn/dT~2.5×10^{-5}) and the Si WG (dn/dT~1.8×10^{-4}), enabling high-fidelity beam-steering in the phased array scanning axis (θ). Another key feature is the Si-Si_3N_4 hybrid grating antenna depicted in Fig.1 (c) with more details provided in our previous work [10]. Owing to the high mode confinement of the silicon WG as well as the low refractive index perturbation of the Si_3N_4 overlayers, centimeter-scale (10.3 mm at a period of 0.7 μm) grating antenna is designed and fabricated without applying ultra-shallow etching or thin-film deposition techniques common in prior arts, resulting in a designed beam divergence of 0.017° in the wavelength scanning axis (ψ). Meanwhile, the two layers of Si_3N_4 perturbations with a longitudinal offset are used to break the symmetry of the grating. Finally, to achieve high resolution and aliasing-free beam-steering at an affordable complexity, the 256 grating antennas are organized into a sparse array of linearly increasing pitches with minimum and maximum pitches of 3.6 and 8.28 μm, respectively. The width of the aperture reaches 1.5 mm, which corresponds to a beam divergence of 0.049 in the phased array scanning axis (θ). A sidelobe suppression ratio (SLSR) of 12 dB is obtained through simulation, which can be further improved to 25 dB with 1000 elements.

3. Laser Characterization and Beam-steering Demonstration

Here we focus on the key specifications of the Tx, including laser performance, beam quality, and beam-steering capability. As shown in Fig. 2 (a), the on-chip output optical power reaches 18.5 mW at a pump current of 420 mA. The maximum power is currently limited by thermal issues including the degradation of RSOA power efficiency and the deformation-induced misalignment between the RSOA and the PIC. Fig. 2 (b) shows the measured optical frequency noise using an optical noise analyzer (SYCATUS, A0040A). The frequency noise levels off at 880 Hz^2/Hz, indicating an intrinsic linewidth of 2.8 kHz. With the single-wavelength continuous-wave operation, after phase alignment at an average TO power consumption of 5 Watt, a high-resolution far-field pattern with a beam divergence of 0.047°(Δθ) × 0.034°(Δψ) is observed in Fig. 2 (c). The beam quality matches the simulation in terms of Δθ (~0.049°), while fabrication-induced uniformity issues degrade the latter Δψ (~0.017°). Nevertheless, both the designed and the demonstrated Δψ break the record achieved on the platform, while Δθ reaches the state-of-the-art at reduced complexity. The SLSR is ~10 dB. Using a remote tunable laser for localized wavelength scanning, the wavelength scanning efficiency is measured to be 0.164°/nm.

To realize beam-steering in the wavelength scanning axis (ψ), we tune one of the MRRs while adjusting the PS and the TSL for mode selection. A wide wavelength tuning range of about 100 nm is achieved as shown in Fig. 2 (d), which corresponds to a beam steering range of ~16°. The side mode suppression ratio of the ECL is more than 42 dB over the tuning range. For beam-steering in the phased array axis (θ), high-fidelity beam orientation without further optimization is demonstrated in Fig. 2 (e) by applying additional phase-shift to each channel based solely on the theoretical phase front sampling of the plane wave that propagates in the target direction. In the worst-case incidence, the maximum deviation between the desired angle and the resolved angle is 0.01° in the phased array scanning axis. An inset in Fig. 2 (e) displays localized two-dimensional beam-steering in a far-field imaging system of high-magnification with an increased noise floor caused by sidelobe superposition. Preliminary beam-steering results indicate that an aliasing-free beam-steering range of 50° × 16° is achievable. The on-chip insertion loss is estimated to be below 3 dB through free-space radiating optical power measurement near the emitting aperture.

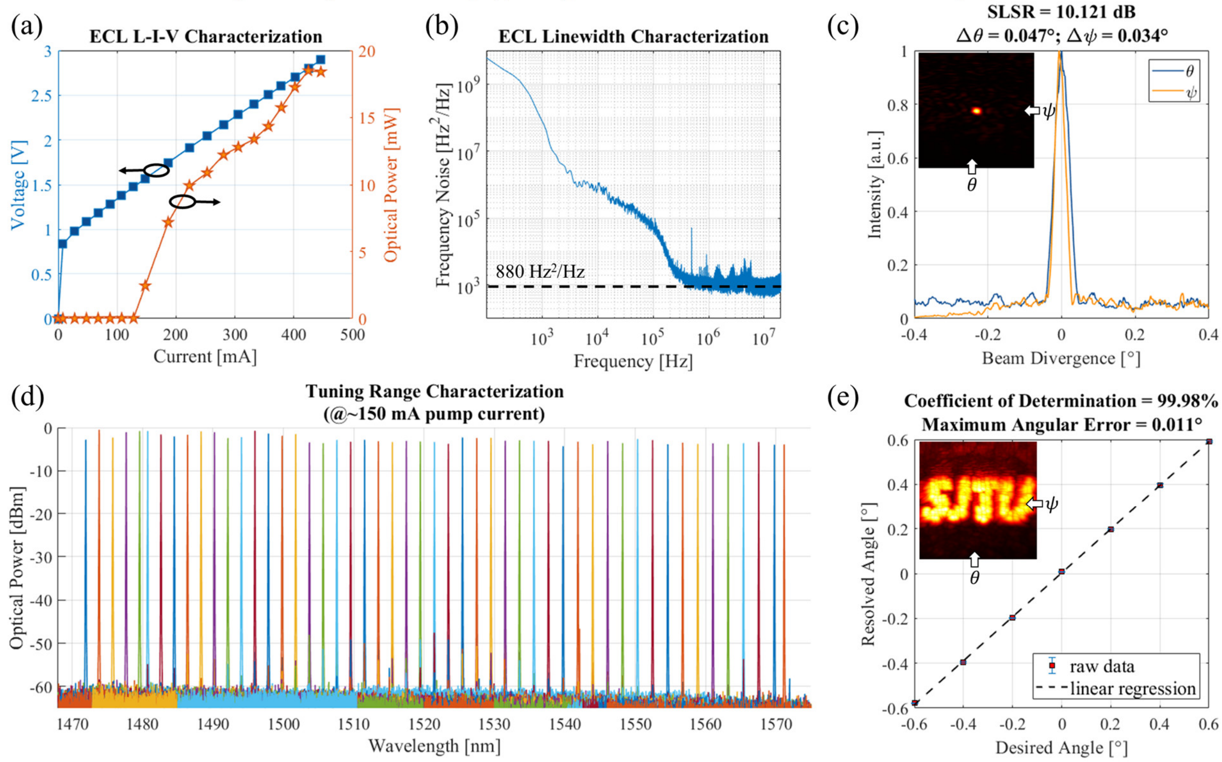

Fig. 2 (a) Measured L-I-V performance of the ECL. (b) Frequency noise spectrum of the ECL. (c) Far-field beam quality characterization of the OPA-based beam-steerer. (d) Superimposed lasing spectra at an RSOA pump current of ~150 mA. (e) Beam-steering fidelity on the phased-array scanning axis (θ), exhibiting high linearity and small deviation and an inset demonstrating 2D beam-steering by scanning the logo *SJTU*.

4. Conclusion

We have demonstrated a fully integrated solid-state LiDAR transmitter on the tri-layer silicon-nitride-on-silicon photonic platform. A tunable narrow-linewidth ECL and a large-scale OPA of record-low insertion loss, high spatial resolution, and accurate beam-steering are achieved in a single PIC at a footprint of 15.6 mm × 11.7 mm. Compared to the prior arts, the silicon-nitride external cavity possesses a high-power threshold in the vernier rings and offers an integrated light source capable of high-power output. Given a higher-gain RSOA, a lower-loss edge coupling, and better thermal dissipation, which is easier to achieve through hybrid integration, the high-power handling capability of silicon nitride waveguides can be fully exploited to provide watt-level optical power to the OPA. Meanwhile, electro-optic or silicon resistive TO phase shifters, as well as germanium-on-silicon photodetectors can be introduced to the OPA, enabling high-speed beam-steering and on-chip phase error correction.

5. References

[1] K. Van Acoleyen, *et al.*, "Off-chip beam steering with a one-dimensional optical phased array on silicon-on-insulator," Opt. Lett. **34**, 1477-1479 (2009).
[2] C. V. Poulton, *et al.*, "8192-element optical phased array with 100° steering range and flip-chip CMOS," in Conference on Lasers and Electro-Optics, OSA Technical Digest (online) (Optical Society of America, 2020), paper JTh4A. 3.
[3] J. Hulme *et al.*, "Fully integrated hybrid silicon two dimensional beam scanner," Optics Express **23**, 5861-5874 (2015).
[4] Y. Zhu, *et al.*, "Hybrid integration of multi-band, tunable external-cavity diode lasers for wide-angle beam steering," in Conference on Lasers and Electro-Optics, OSA Technical Digest (online) (Optical Society of America, 2019), 1-2.
[5] S.-M. Kim, *et al.*, "Compact solid-state optical phased array beam scanners based on polymeric photonic integrated circuits," Scientific Reports **11**, paper 10576 (2021).
[6] W. D. Sacher *et al.*, "Tri-layer silicon nitride-on-silicon photonic platform for ultra-low-loss crossings and interlayer transitions," Optics Express **25**, 30862-30875 (2017).
[7] L. Zhang *et al.*, "Investigation and demonstration of a high-power handling and large-range steering optical phased array chip," Optics Express **29**, 29755-29765 (2021).
[8] Q. Wilmart *et al.*, "A versatile silicon-silicon nitride photonics platform for enhanced functionalities and applications," Applied Sciences **9**, paper 255 (2019).
[9] Q. Wang, *et al.*, "Silicon nitride assisted 1×64 optical phased array based on a SOI platform," Optics Express **29**, 10509-10517 (2021).
[10] W. Xu *et al.*, "Impact of Aperture Size on Beam Evolution of Optical Phased Arrays," in Optical Fiber Communication Conference, OSA Technical Digest (online) (Optical Society of America, 2021), paper F4A.4.